論文 / 著書情報
Article / Book Information

論題	
Title	Surface modification of Y2O3:Er,Yb upconversion nanoparticles prepared by laser ablation in water
著者	小林 光, 藤井 邦生, 布川 貴史, 小田原 修, 和田 裕之
Authors	Hikaru Kobayashi, Kunio Fujii, Takashi Nunokawa, Osamu Odawara, Hiroyuki Wada
出典	, vol. 53, num. 5S1,
Citation	Japanese Journal of Applied Physics, vol. 53, num. 5S1,
発行日 / Pub. date	2014, 5
DOI	http://dx.doi.org/10.7567/JJAP.53.05FK04
URL	http://dx.doi.org/10.7567/JJAP.53.05FK04
権利情報 / Copyright	本著作物の著作権は（公社）応用物理学会に帰属します。 (c) 2014 The Japan Society of Applied Physics
Note	このファイルは著者（最終）版です。 This file is author (final) version.

doi:10.7567/JJAP.53.05FK04
Japanese Journal of Applied Physics

Surface modification of Y_2O_3:Er,Yb upconversion nanoparticles prepared by laser ablation in water

Hikaru Kobayashi, Kunio Fujii, Takashi Nunokawa, Osamu Odawara, and Hiroyuki Wada*

Tokyo Institute of Technology, Yokohama 226-8502, Japan

E-mail: wada.h.ac@m.titech.ac.jp

doi:10.7567/JJAP.53.05FK04
Japanese Journal of Applied Physics

Abstract:

Y_2O_3:Er,Yb upconversion nanoparticles were prepared by laser ablation in liquid and capped with poly(ethylene glycol) (PEG). A Nd:YAG green laser with nanosecond pulse duration was used. Capping was carried out by a two-step process. The first step is surface modification using a silane coupling agent, (3-aminopropyl)triethoxysilane (APTES), to aminate the surface of nanoparticles. The second step was the conjugation of PEG chains to the surface by amido binding reaction between the surface amino groups and activated esters connected to PEG. The prepared upconversion nanoparticles were highly crystalline polycrystals, the particle size of which was approximately 20 nm. Dopants in phosphor nanoparticles were not removed by laser irradiation. The spectra of PEG-capped nanoparticles were almost the same as those of uncapped nanoparticles. The capped nanoparticles would be useful for biomedical applications.

doi:10.7567/JJAP.53.05FK04
Japanese Journal of Applied Physics

1. Introduction

Over the past several years, there has been increasing interest in upconversion materials owing to their unique properties and various applications in research fields, such as biotechnology and electronics. Upconversion materials can be excited by infrared (IR) light, which has a lower energy than visible emission light.[1-5] In biomedical research, there is light absorption in a living body in the visible region due to hemoglobin and in the far-IR region due to water.[6] Because of less absorption in the near-IR region, which is called the 'optical window,' bioimaging and cancer therapy using upconversion nanoparticles have been studied. Usually, the inside of a living body is examined by opening the abdominal cavity. The advantage of upconversion nanoparticle is bioimaging without requiring the surgical operation of a living body. Another potential application is cancer therapy. Photodynamic therapy (PDT) is one of the less-invasive therapies, by which reactive oxygen species are generated in cancer cells by irradiating a photosensitizer with visible light. The disadvantage of this therapy is the difficulty in curing large cancer and deeply placed cancer owing to the low transparency of visible light. The combination of the use of upconversion nanoparticles and irradiation with IR light may solve the above-mentioned problems.[7-11] For these applications, particle size is important. From the viewpoint of long residence time of nanoparticles in blood vessels, a particle size in the range between about 10 and 200 nm is needed because particles with a

diameter larger than 200 nm are accumulated in Kupffer cells in the liver[12] and those smaller than about 10 nm are egested from the kidney.[13] From the viewpoint of cancer, particles smaller than 200 nm target tumors passively owing to the enhanced permeability and retention (EPR) effect.[14] Although $NaYF_4$:Er,Yb is widely studied as an upconversion material owing to its low phonon energy,[15-17] some researchers are concerned about the toxicity of fluorine. Y_2O_3:Er,Yb is also one of the typical upconversion materials[18,19] with high stability and comparatively low phonon energy.[20]

For biomedical applications, the capping of nanoparticles is one of the important issues. When a ceramic nanoparticle exists in a living body, nonspecific adhesion occurs. To prevent this phenomenon, the capping of a nanoparticle with a biocompatible layer such as poly(ethylene glycol) (PEG) would be required.[21-23] The capping layer would also prevent aggregation of nanoparticles induced by the steric effect.[24]

One of the promising methods to prepare nanoparticles is laser ablation in liquid. This method was first used for analysis.[25] However, it has been used for generation of nanoparticles in liquid recently.[26-29] By using this method for ceramics materials such as doped phosphor, highly crystalline multielement nanoparticles can be obtained.[30-33]

In this study, laser ablation in liquid was applied to the preparation of Y_2O_3:Er,Yb nanoparticles capped with PEG. The optical properties were studied. Previously, we capped

nanoparticles with PEG by physical adsorption.[34-36] However, the force of physical adsorption would be weaker than that of chemical adsorption. In this study, chemical adsorption was achieved by reaction with a silane coupling agent.

2. Experimental methods

Y_2O_3:Er,Yb nanoparticles were prepared by laser ablation in liquid. The target of laser ablation in liquid was synthesized by the coprecipitation method. Yttrium nitrate hexahydrate, erbium nitrate pentahydrate, and ytterbium nitrate hydrate were dissolved in de-ionized (DI) water (50 ml). Sodium carbonate aqueous solution (50 ml) was added to the solution, which was then stirred for 2 h. The precipitate as a precursor was washed with DI water and separated by centrifugation (3000 rpm) three times. It was dried at 60 °C for 12 h. The precursor ground using mortar and pestle was calcined in an electric furnace at 900 °C for 30 min to synthesize Y_2O_3:Er,Yb. The particles were pressed at a pressure of 200 MPa for 6 min to form a pellet. The pellet was sintered at 1200 °C for 2 h in air to obtain the laser ablation target. The target was irradiated in DI water (3 ml) with a focused pulse laser beam (Nd:YAG/SHG; wavelength, 532 nm; repetition rate, 10 Hz; pulse duration, 13 ns) for 5 min. The irradiated area on the target was 0.10 mm^2. The energy of the laser was varied in the range from 3.9 to 91.0 mJ/pulse.

The nanoparticles (39 J/cm^2) were capped with a silane coupling agent

(3-aminopropyl)triethoxysilane (APTES) and then with PEG similarly to a previous study.[23] The nanoparticles (2 mg) were ultrasonically dispersed in 2-propanol (2 ml) for 15 min. APTES (1.2 μl) was added to the solution and stirred at 70 °C for 24 h to obtain APTES-capped upconversion nanoparticles, on the surface of which amino groups existed. The nanoparticles were washed with 2-propanol and separated by centrifugation (14000 rpm) three times. They were dried in a vacuum oven to obtain the powder form of APTES-capped upconversion nanoparticles (Y_2O_3:Er,Yb-APTES). The powder (2 mg) was ultrasonically dispersed in dimethyl sulfoxide (DMSO). *N*-Hydroxysuccinimide-PEG (NHS-PEG) with activated ester was added to the solution and then stirred at room temperature for 24 h. The sample in the solution was separated by centrifugation (14000 rpm) and washed with DMSO three times. The sample was dried in a vacuum oven to obtain the powder of PEG-capped upconversion nanoparticles (Y_2O_3:Er,Yb-PEG).

The nanoparticles were identified by X-ray diffraction (XRD) analysis. Particle size and morphology were examined by scanning electron microscopy (SEM) and transmission electron microscopy (TEM). The solution with nanoparticles dispersed was dropped onto a carbon membrane on a copper grid, and the solvent was removed by drying in a vacuum oven. The elements of nanoparticles were analyzed by energy dispersive X-ray (EDX) spectroscopy. Capped nanoparticles were analyzed by Fourier transform infrared spectroscopy (FT-IR). The

KBr pellet method (0.2 wt%) was used to prepare sample for the measurement. The upconversion spectra of the solution with nanoparticles dispersed were measured using a fluorescence spectrophotometer at room temperature. A laser diode (LD; wavelength, 980 nm) was used for excitation. The turbidity of the solution with nanoparticles dispersed was measured using a spectrophotometer.

3. Results and discussion

XRD analysis was carried out to examine the powder prepared by laser ablation in liquid. The XRD patterns of the target and nanoparticles are shown in Fig. 1. The patterns indicate that the prepared powder was Y_2O_3 (space group: *Ia*-3, No. 206), which was the target of laser ablation in liquid. By-products were not observed in the powder. Because the melting point of Y_2O_3 is high, the reaction between the target and the solvent did not occur during laser ablation.

The particle size of prepared powder was measured by SEM as shown in Fig. 2. The laser energy densities on the target during laser ablation in liquid for nanoparticles shown in Figs. 2(a)-2(c) were 3.8, 38, and 50 J/cm^2, respectively. Figure 2(d) shows the target. Nanoparticles were prepared at a low laser energy density, while nanostrings were prepared at a high laser energy density. The nanoparticles shown in Figs. 2(a)-2(b) were smaller than the primary particles of the target, as shown in Fig. 2(d). The primary particles in the target would fragment

into fine nanoparticles following the laser irradiation, the average particle size of which was 14.9 nm. The nanostrings shown in Fig. 2(c) were considered to have been formed following the melting of aggregated nanoparticles due to heat of laser pulses, because the diameter of the nanostrings was almost the same as that of the nanoparticles. The probability of aggregation of nanoparticles is high at a high concentration of nanoparticles. At a high laser energy density, the concentration of the prepared nanoparticles was high. Therefore, the nanostrings would be formed, as shown in Fig. 2(c). From the results of XRD analysis and SEM, upconversion nanoparticles were successfully prepared by laser ablation in liquid.

The average particle sizes of nanoparticles prepared at various laser energy densities are shown in Fig. 3. The particle size gradually increased with increasing energy density. A similar tendency was observed previously.[31)] The nanoparticles would be formed in plasma plume during laser ablation. The amount of emitted atoms, ions, and clusters during laser ablation would increase with increasing energy density of the irradiated laser beam. The increase in the amount of chemical species would increase the concentration of the species in plume, thereby inducing the crystal growth of nanoparticles. Therefore, the increase in particle size would be observed.

The size distributions of the nanoparticles shown in Figs. 2(a) and 2(b) are shown in Figs. 4(a) and 4(b), respectively. Figure 4(a) shows a bimodal distribution, which indicates the

existence of both small and large nanoparticles, while Fig. 4(b) shows a monomodal distribution. The increasing laser energy density decreased the number of small nanoparticles. In laser plume, small nanoparticles would be absorbed by large nanoparticles at a high temperature, resulting in the increase in average particle size from 14.9 to 18.3 nm.

Figure 5 shows TEM images of an APTES-capped upconversion nanoparticle. The inset shows an enlarged view of the nanoparticle. The nanoparticle was almost spherical, and lattice fringes indicated the high crystallinity of the nanoparticles. The various directions of the lattice fringes in a nanoparticle indicate that one nanoparticle consists of small nanoparticles that melted after the irradiation with a pulse laser beam. This hypothesis is supported by the increase in particle size shown in Fig. 3 and the particle size distribution in Fig. 4. These polycrystalline nanoparticles can likely be prepared at a higher laser energy density. The inset in Fig. 5 shows a lattice spacing of 3.054 Å, which almost corresponds to the lattice spacing of the (222) plane of the Y_2O_3 matrix, which shows the strongest peak of XRD.

Figure 6 shows the EDX data of APTES-capped upconversion nanoparticles. It indicated the existence of the elements of the Y_2O_3 matrix and its dopants Er and Yb in nanoparticles. No complete evaporation of dopant occurred. The easy preparation of multielement nanoparticles is the advantage of laser ablation in liquid. The peak of Si was attributed to APTES. The peak of Cu was attributed to the grid for TEM observation.

The FT-IR spectrum of APTES-capped nanoparticles is shown in Fig. 7. The stretching mode of C-C bonding is observed at 2900 cm^{-1}.[23,37] The asymmetric stretching mode of C-O-C bonding is observed at 1100 cm^{-1}.[23,37] These peaks in Fig. 7 would correspond to the PEG chain. The nanoparticles would be capped with PEG by the linkage of APTES. The amino group NH_2 would exist on the surface of an APTES-capped nanoparticle. The amino group and activated ester in *N*-hydroxysuccinimide-PEG reacted by amide binding and then PEG would conjugate with the surface of the nanoparticle. The peaks at 3400, 2400, and 1600 cm^{-1} were attributed to OH, CO_2, and H_2O, respectively.

Figure 8 shows the upconversion spectra of Y_2O_3:Er,Yb nanoparticles, APTES-capped Y_2O_3:Er,Yb nanoparticles, and PEG-capped Y_2O_3:Er,Yb. The spectral shapes are almost same. Capping did not affect optical properties. Therefore, capped nanoparticles can be used in various applications. The energy diagrams of Er^{3+} and Yb^{3+} ions are shown in Fig. 9. The strong red emission is attributed to the following processes:

$^4I_{15/2} \rightarrow {}^4I_{11/2}$,

$^4I_{11/2} \rightarrow {}^4I_{13/2}$ (nonradiative relaxation) ,

$^4I_{13/2} \rightarrow {}^4F_{9/2}$,

$^4F_{9/2} \rightarrow {}^4I_{15/2}$.

In contrast, the green emission is attributed to the following processes:

$^4I_{15/2} \rightarrow {}^4I_{11/2}$,

$^4I_{11/2} \rightarrow {}^2H_{11/2}/{}^4S_{3/2}$,

$^2H_{11/2}/{}^4S_{3/2} \rightarrow {}^4I_{15/2}$.

In general, a nanoparticle has a large specific surface area, which would enhance nonradiative relaxation through surface defects and/or energy transfer to water molecules. The increase in nonradiative relaxation would increase the ratio of red emission to green emission, which included nonradiative relaxation. The red emission is useful in biomedical fields owing to the high transparency of a living body.

Figure 10 shows the turbidity of the solution with nanoparticles dispersed as a function of time. Because absorbance is proportional to the concentration of nanoparticles according to the Lambert-Beer law, the turbidity T is defined as follows:

$$T = A / A_0 \times 100,$$

where A is the absorbance and A_0 is the initial absorbance. In general, the precipitation of nanoparticles due to aggregation decreases the concentration of nanoparticles at the light path and then the turbidity also decreases. The turbidity of Y_2O_3:Er,Yb-PEG nanoparticles was stable, while those of Y_2O_3:Er,Yb-APTES and Y_2O_3:Er,Yb nanoparticles decreased gradually. In general, the stability of the solution with nanoparticles dispersed is improved by the electrostatic and steric effects.[24] In this study, the steric effect of the PEG chain increased the stability of

upconversion nanoparticle solution, which is important for biomedical applications.

4. Conclusions

We prepared highly crystalline upconversion nanoparticles dispersed in water by laser ablation in liquid. Nanoparticles were prepared at a low laser energy density, while nanostrings were prepared at a high laser energy density. Particle size increased with increasing irradiated laser energy density. The crystallinity of nanoparticles was high and the prepared nanoparticles were polycrystalline. Doped ions existed in the nanoparticles prepared by laser ablation, although we were concerned about the evaporation of dopants. Upconversion nanoparticles were capped with PEG by silane coupling. Regarding the spectra of upconversion nanoparticles in this measurement, red emission was stronger than green emission. Spectral shape was not affected by PEG capping. The dispersibility of upconversion nanoparticles was improved by the PEG-capping-induced steric effect. Highly crystalline upconversion nanoparticles capped with PEG were successfully obtained.

Acknowledgements

The authors wish to thank Professors K. Nakamura (laser ablation), T. Yamaguchi (SEM), and T. Tsuge (spectrophotometer), Specialists K. Hori (TEM), H. Iida (XRD), and M. Tada

(FT-IR) of Tokyo Tech. This study was supported by a JSPS KAKENHI Grant Number 25390014 and the Collaborative Research Project of Materials and Structures Laboratory.

References

1) F. Auzel, Chem. Rev. **104**, 139 (2004).

2) F. Auzel, C. R. Acad. Sci. (Paris) **262**, 1016 (1966) [in French].

3) F. Auzel, C. R. Acad. Sci. (Paris) **263**, 819 (1966) [in French].

4) V. Ovsyankin, and P. P. Feofilov, JETP Lett. **3**, 317 (1966).

5) V. Ovsyankin, and P. P. Feofilov, JETP Lett. **3**, 322 (1966).

6) M. S. Patterson, B. C. Wilson, and D. R. Wyman, Lasers Med. Sci. **6**, 379 (1991).

7) P. Zhang, W. Steelant, M. Kumar, and M. Scholfield, J. Am. Chem. Soc. **129**, 4526 (2007).

8) Y. Y. Guo, M. Kumar, and P. Zhang, Chem. Mater. **19**, 6071 (2007).

9) H. S. Qian, H. C. Guo, P. C. L. Ho, R. Mahendran, and Y. Zhang, Small, **5**, 2285 (2009).

10) J. N. Shan, S. J. Budijono, G. H. Hu, N. Yao, Y. B. Kang, Y. G. Ju, and R. K. Prud'homme, Adv. Funct. Mater. **21**, 2488 (2011).

11) C. Wang, H. Q. Tao, L. Cheng, and Z. Liu, Biomaterials, **32**, 6145 (2011).

12) A. Schadlich, H. Caysa, T. Mueller, F. Tenambergen, C. Rose, A. Gopferich, J. Kuntsche, and K. Mader, ACS Nano, **5**, 8710 (2011).

13) M. Ohlson, J. Sorensson, and B. Haraldsson, Am. J. Physiol. Renal Physiol. **280**, F396 (2001).

14) Y. Matsumura, and H. Maeda, Cancer Res. **46**, 6387 (1986).

15) S. Heer, K. Kompe, H. U. Gudel, and M. Haase, Adv. Mater. **16**, 2102 (2004).

16) X. Wang, J. Zhuang, Q. Peng, and Y. Li, Nature, **437**, 121 (2005).

17) Y. Wei, F. Lu, X. Zhang, and D. Chen, Chem. Mater. **18**, 5733 (2006).

18) M. Kamimura, D. Miyamoto, Y. Saito, K. Soga, and Y. Nagasaki, Langmuir, **24**, 8864 (2008).

19) T. Zako, H. Nagata, N. Terada, A. Utsumi, M. Sakono, M. Yohda, H. Ueda, K. Soga, and M. Maeda, Biochem. Biophys. Res. Commun. **381**, 54 (2009).

20) T. T. Basiev, A. Y. Dergachev, Y. V. Orlovsky, V. V.Osiko, and A. M. Prokhorov, Bull. Russ. Acad. Sci. Phys. **56**, 219 (1992).

21) K. Uchida, H. Otsuka, M. Kaneko, K. Kataoka, and Y. Nagasaki, Anal. Chem. **77**, 1075 (2005).

22) J. Blummela, N. Perschmann, D. Aydin, J. Drinjakovic, T. Surrey, M. Lopez-Garcia, H. Kessler, and J. P. Spatz, Biomaterials, **28**, 4739 (2007).

23) T. Zako, H. Nagata, N. Terada, M. Sakono, K. Soga, and M. Maeda, J. Mater. Sci. **43**, 5325 (2008).

24) G. Gao, *Nanostructures and Nanomaterials* (Imperial College Press, London, 2004) Chap. 2.

25) P. P. Patil, D. M. Phase, S. A. Kulkarni, S. V. Ghaisas, S. K. Kulkarni, S. M. Kanetkar, and S. B. Ogale, Phys. Rev. Lett. **58**, 3 (1987).

26) F. Mafune, J. Y. Kohno, Y. Takeda, T. Kondow, and H. Sawabe, J. Phys. Chem. B, **104**, 8333 (2000).

27) Y. Tamaki, T. Asahi, and H. Masuhara, Appl. Surf. Sci. **168**, 85 (2000).

28) H. Usui, Y. Shimizu, T. Sasaki, and N. Koshizaki: J. Phys. Chem. B, **109**, 120 (2005).

29) C. L. Sajti, R. Sattari, B. N. Chichkov, and S. Barcikowski: J. Phys. Chem. C, **114**, 2421 (2010).

30) T. Nunokawa, Y. Onodera, M. Hara, Y. Kitamoto, O. Odawara, and H. Wada, Appl. Surf. Sci. **261**, 118 (2012).

31) Y. Onodera, T. Nunokawa, O. Odawara, and H. Wada, J. Lumi. **137**, 220 (2013).

32) Y. Onodera, T. Nunokawa, O. Odawara, and H. Wada, Trans. Mater. Res. Soc. Jpn. **38**, 145 (2013).

33) T. Nunokawa, Y. Onodera, H. Kobayashi, T. Asahi, O. Odawara, and H. Wada, J. Ceram. Process. Res. **14**, s1 (2013).

34) S. Tachikawa, A. Noguchi, M. Hara, O. Odawara, and H. Wada, J. Ceram. Process. Res. **12**,

s215 (2011).

35) S. Tachikawa , A. Noguchi , T. Tsuge , M. Hara , O. Odawara, and H. Wada, Materials, **4**, 1132 (2011).

36) F. Yoshimura, M. Ishizaki, F. Wakai, M. Hara, O. Odawara, and H. Wada, Adv. Opt. Technol. **2012**, 814745 (2012).

37) R. D. Palma, S. Peeters, M. J. V. Bael, H. V. Rul, K. Bonroy, W. Laureyn, J. Mullens, G. Borghs, and G. Maes, Chem. Mater. **19**, 1821 (2007).

Figure captions

Fig. 1. XRD patterns of (a) target and (b) nanoparticles.

Fig. 2. SEM images of nanoparticles [energy densities: (a) 3.8 J/cm^2, (b) 38 J/cm^2 and (c) 50 J/cm^2] and (d) target.

Fig. 3. Average particle size as a function of energy density.

Fig. 4. Particle size distribution at different energy densities [energy densities: (a) 3.8 J/cm^2 and (b) 38 J/cm^2].

Fig. 5. TEM images of nanoparticle capped with APTES (energy density: 39 J/cm^2).

Fig. 6. EDX data of APTES-capped upconversion nanoparticles (energy density: 39 J/cm^2).

Fig. 7. FT-IR spectra of Y_2O_3:Er,Yb nanoparticles capped with PEG.

doi:10.7567/JJAP.53.05FK04
Japanese Journal of Applied Physics

Fig. 8. Upconversion spectra of nanoparticles. (a) Y_2O_3:Er,Yb, (b) Y_2O_3:Er,Yb-APTES, (c) Y_2O_3:Er,Yb-PEG.

Fig. 9. Energy diagram of Er and Yb.

Fig. 10. Turbidity as a function of time. (a) Y_2O_3:Er,Yb-PEG, (b) Y_2O_3:Er,Yb-APTES, (c) Y_2O_3:Er,Yb.

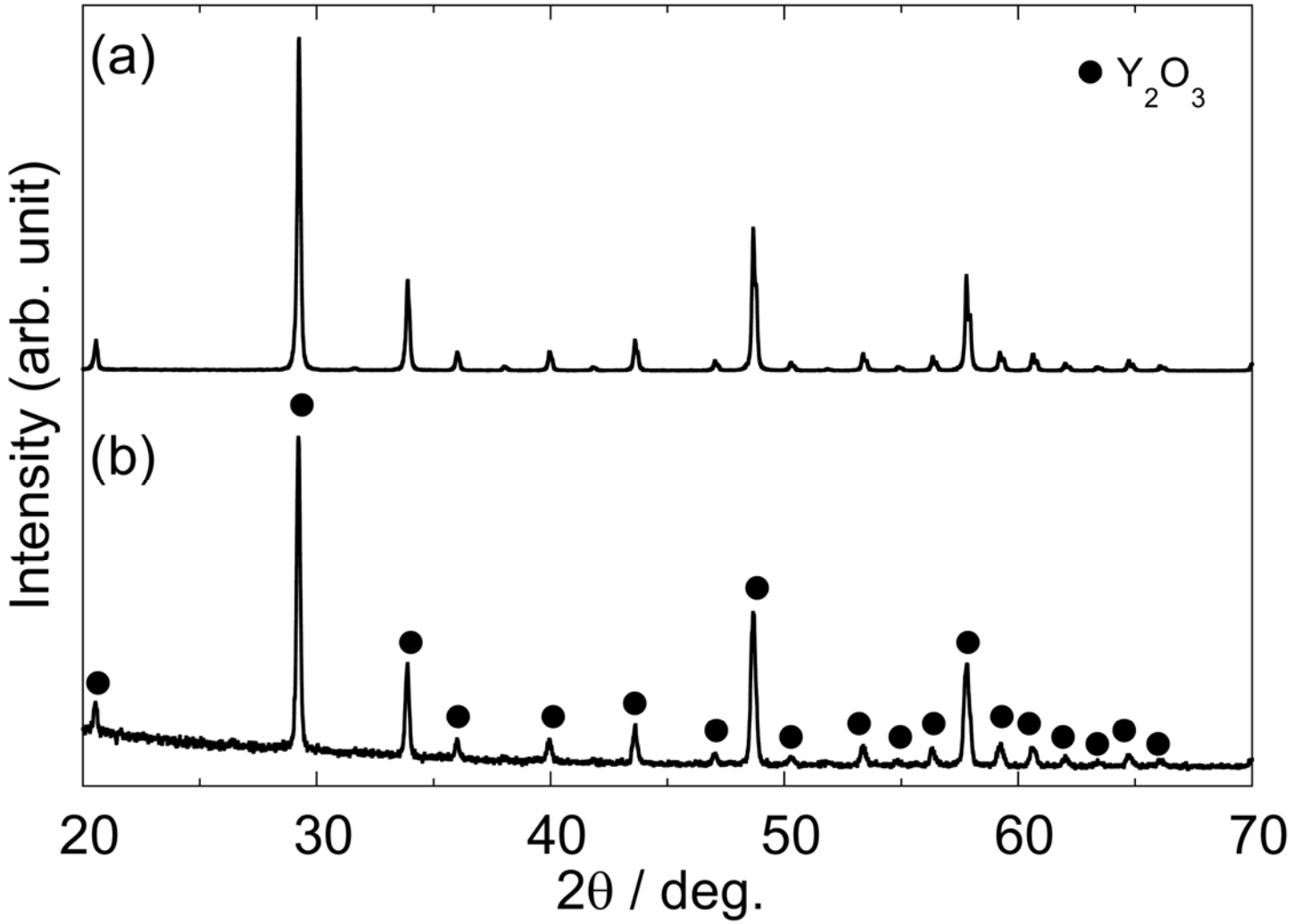

Fig. 1. XRD patterns of (a) target and (b) nanoparticles.

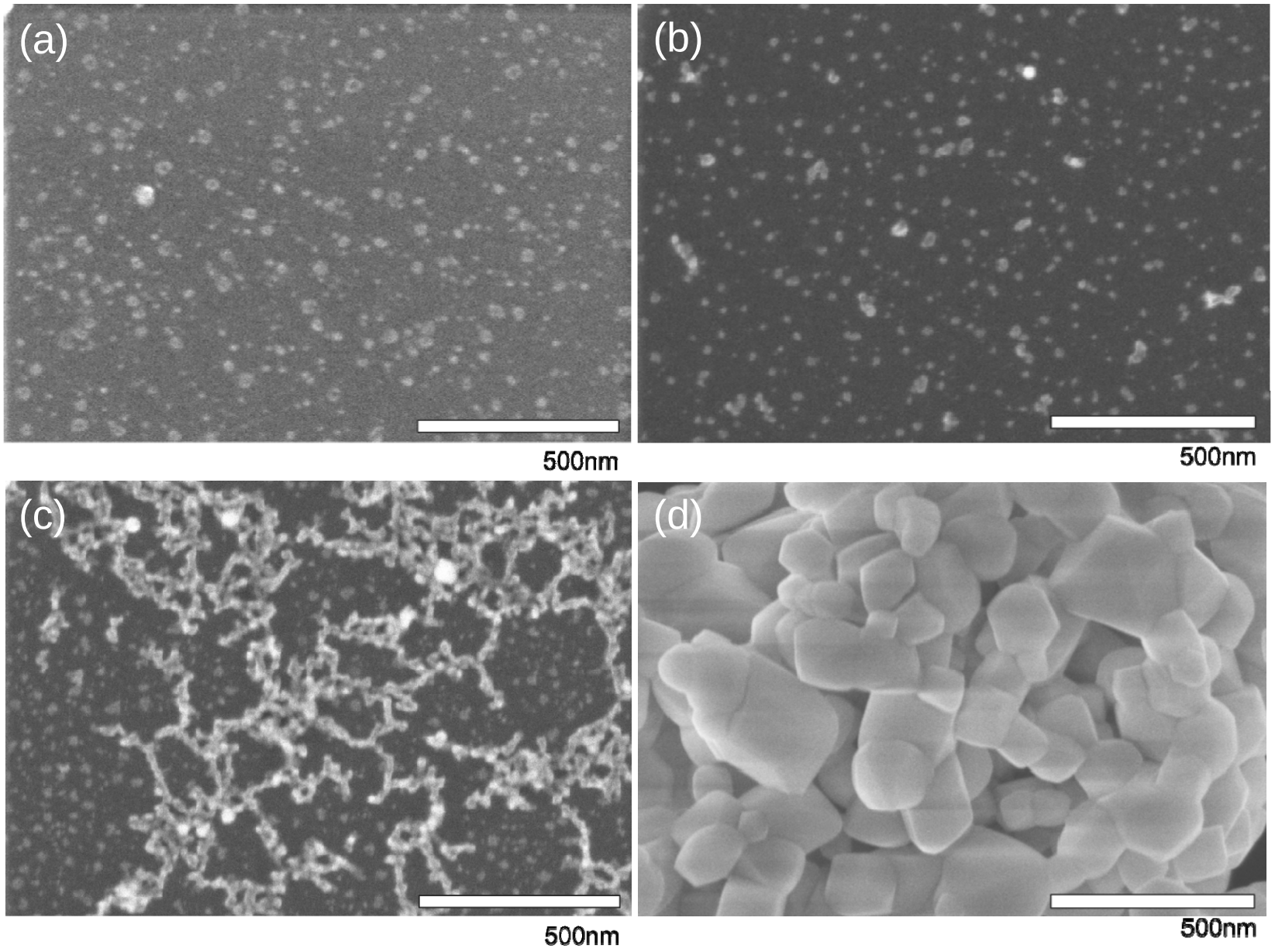

Fig. 2. SEM images of nanoparticles [energy densities: (a) 3.8 J/cm^2, (b) 38 J/cm^2 and (c) 50 J/cm^2] and (d) target.

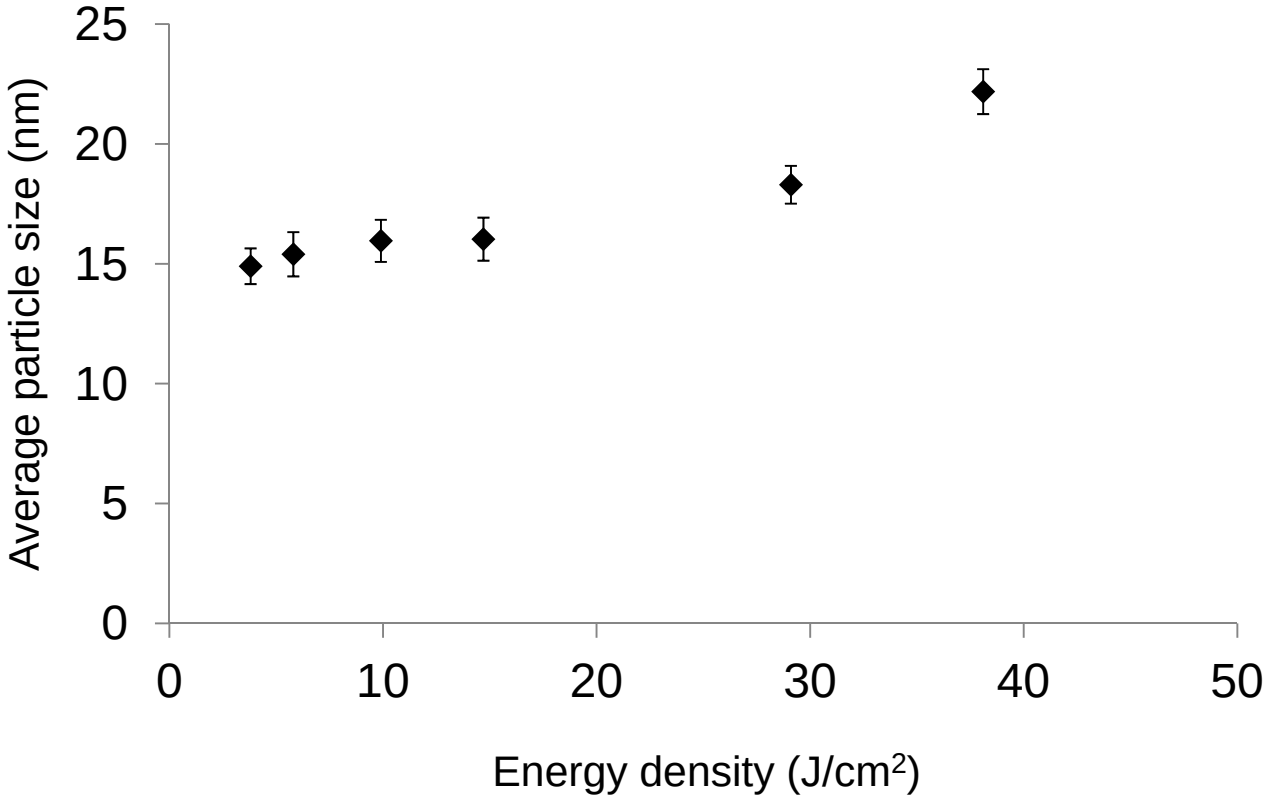

Fig. 3. Average particle size as a function of energy density.

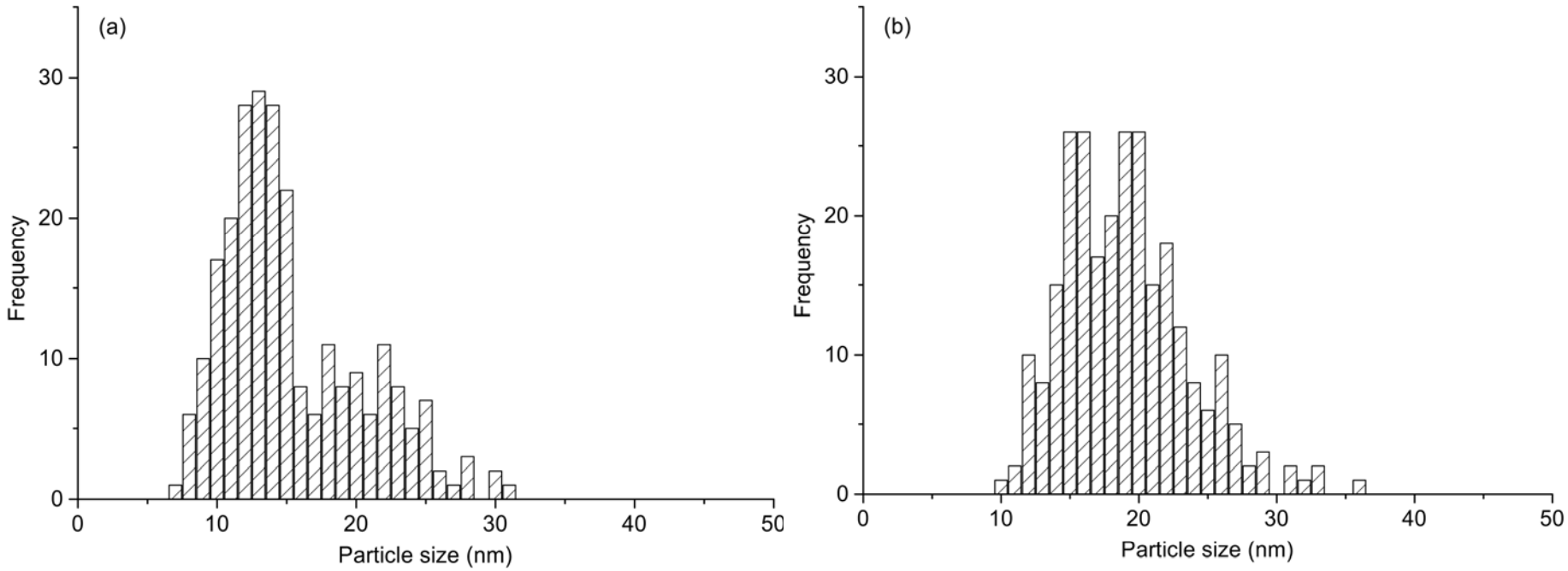

Fig. 4. Particle size distribution at different energy densities [energy densities: (a) 3.8 J/cm^2 and (b) 38 J/cm^2].

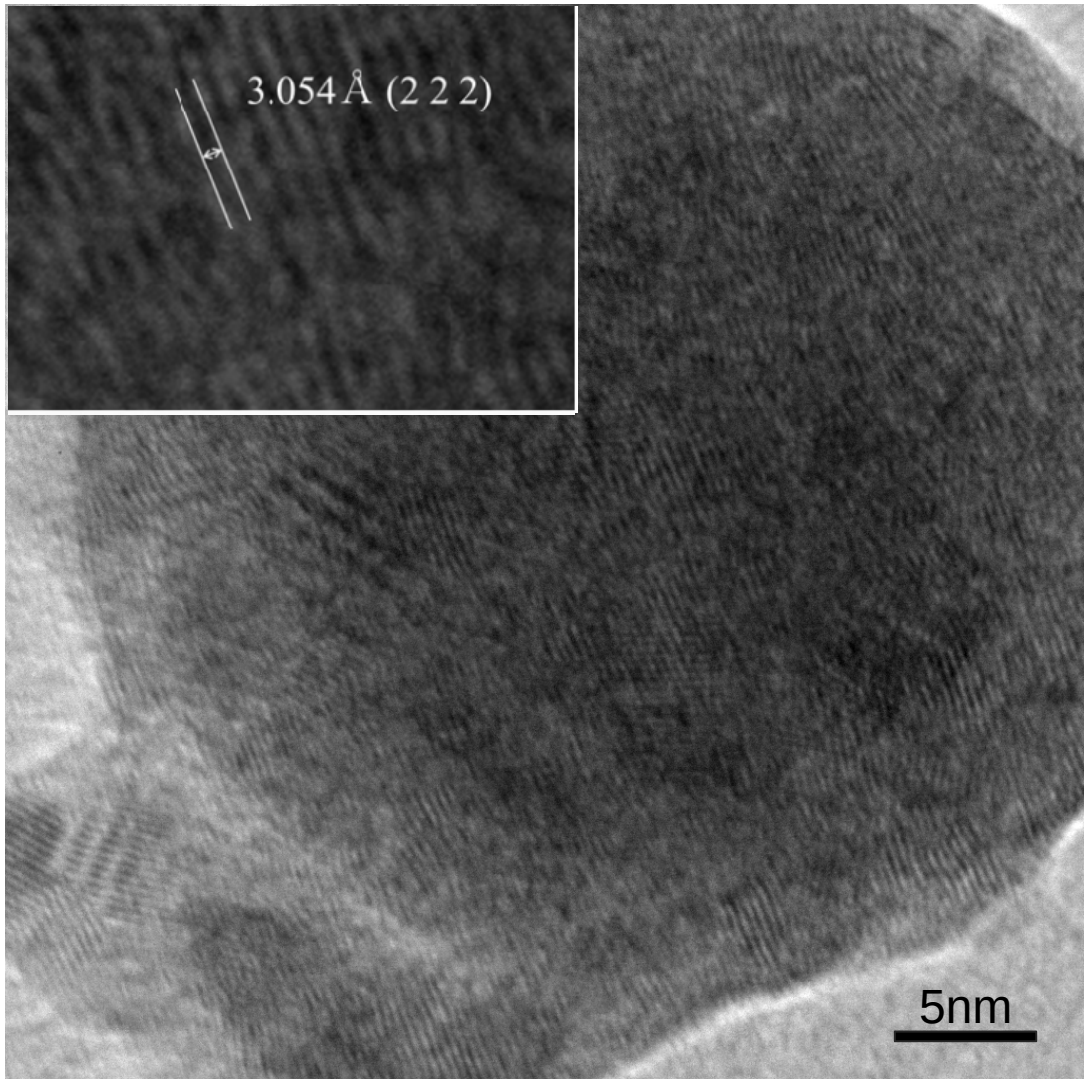

Fig. 5. TEM images of nanoparticle capped with APTES (energy density: 39 J/cm^2).

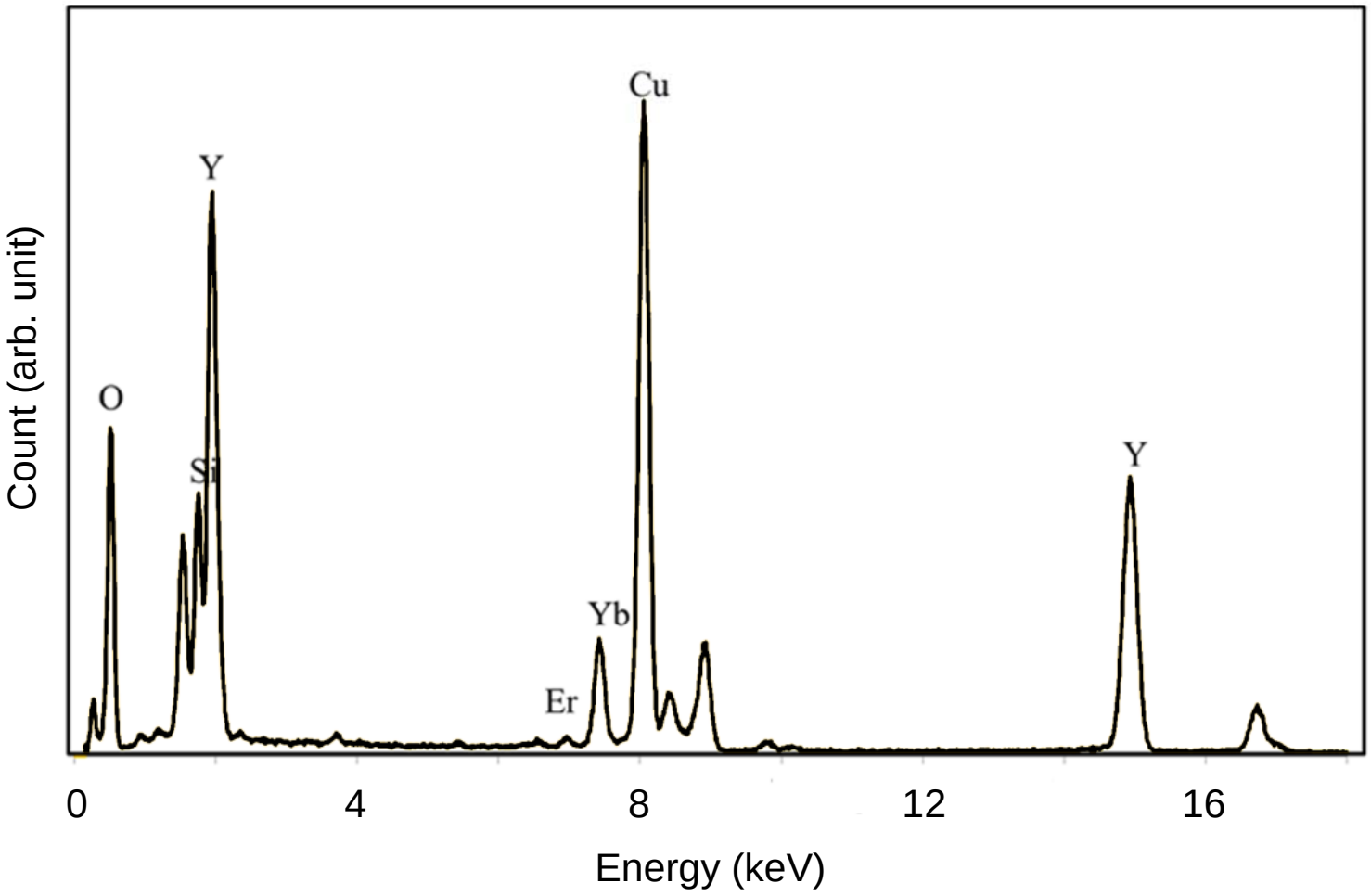

Fig. 6. EDX data of APTES-capped upconversion nanoparticles (energy density: 39 J/cm^2).

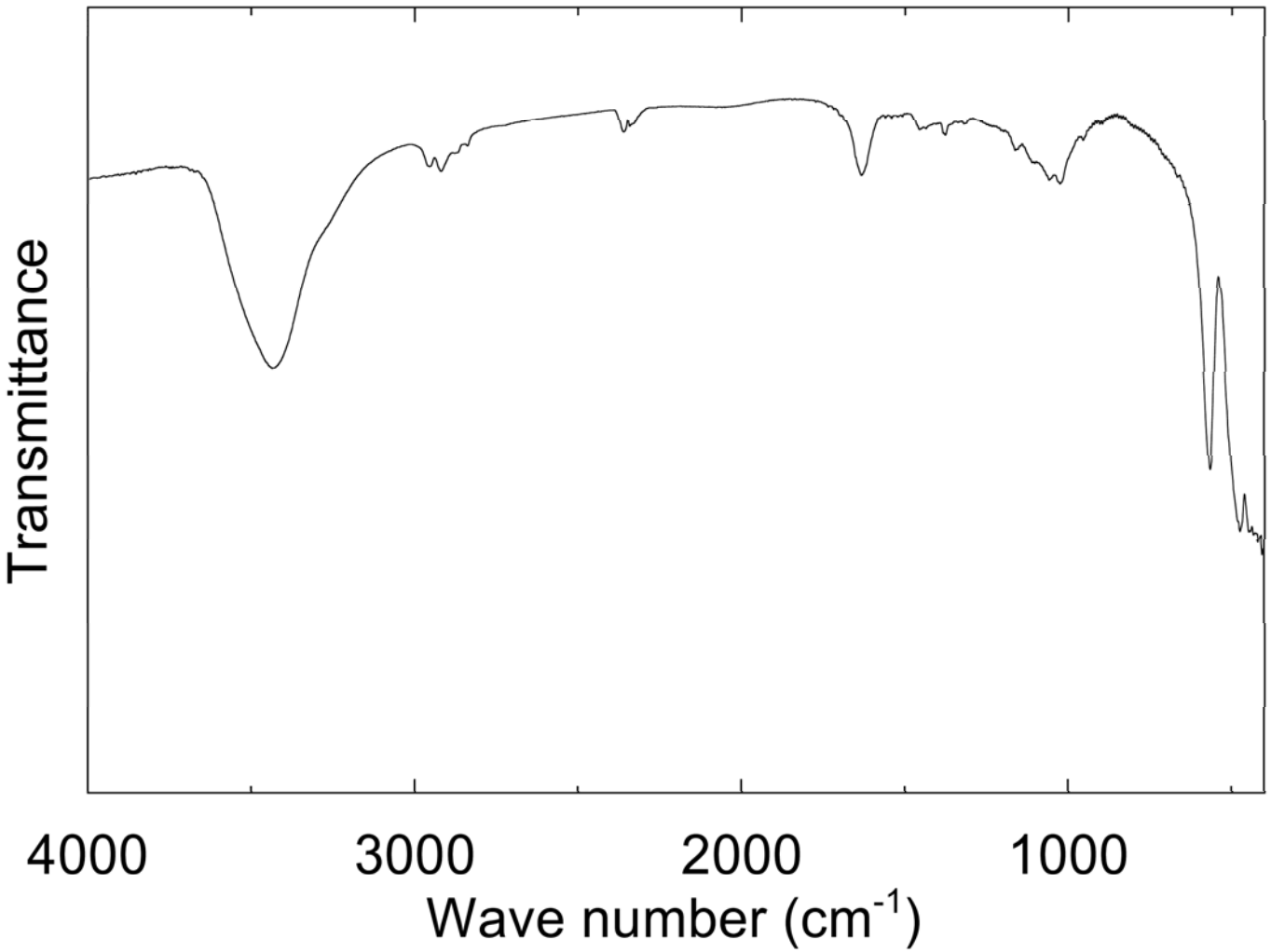

Fig. 7. FT-IR spectra of Y_2O_3:Er,Yb nanoparticles capped with PEG.

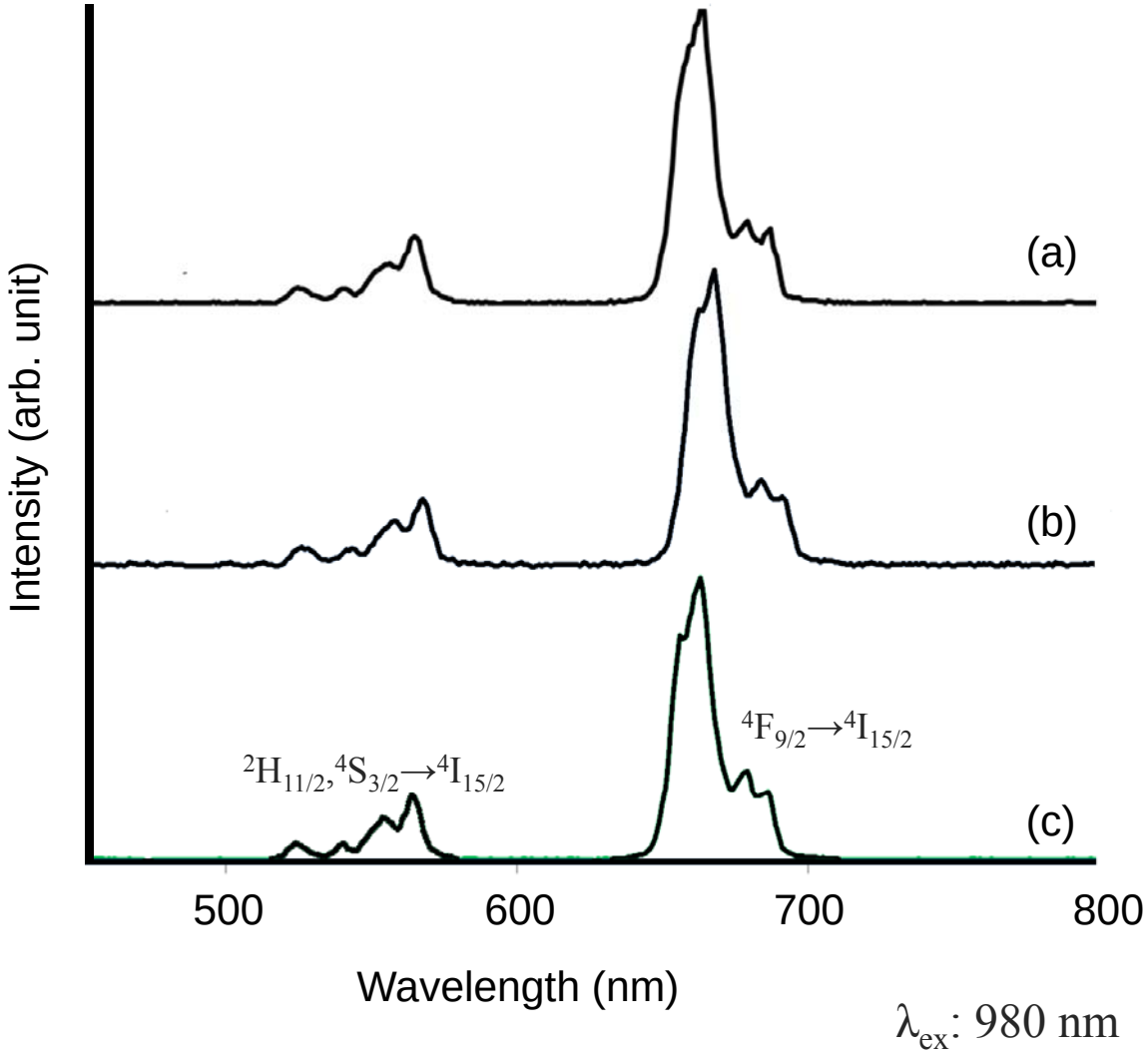

Fig. 8. Upconversion spectra of nanoparticles. (a) Y_2O_3:Er,Yb, (b) Y_2O_3:Er,Yb-APTES, (c) Y_2O_3:Er,Yb-PEG.

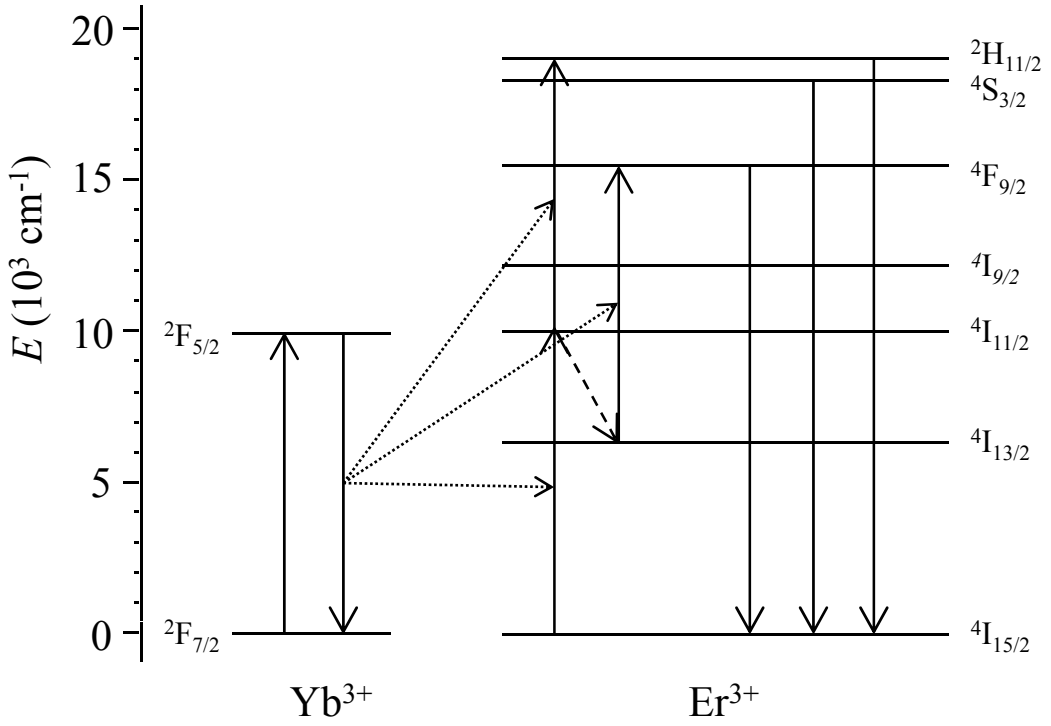

Fig. 9. Energy diagram of Er and Yb.

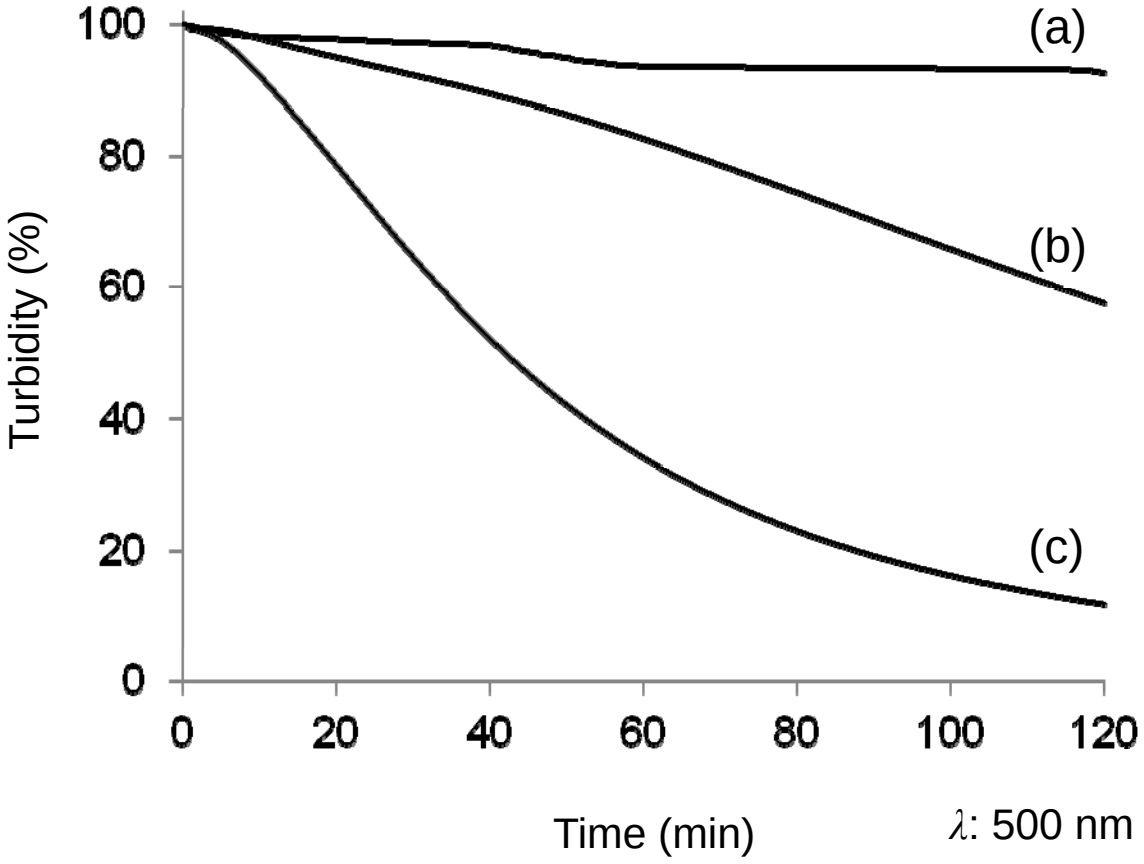

Fig. 10. Turbidity as a function of time. (a) Y_2O_3:Er,Yb-PEG, (b) Y_2O_3:Er,Yb-APTES, (c) Y_2O_3:Er,Yb.